Numerical Prediction of the 10–11 June 1985 Squall Line with the Canadian Regional Finite-Element Model

STÉPHANE BÉLAIR AND DA-LIN ZHANG

Department of Atmospheric and Oceanic Sciences, McGill University, Montreal, Quebec, Canada

JOCELYN MAILHOT

Recherche en Prévision Numérique, Atmospheric Environment Service, Dorval, Quebec, Canada

(Manuscript received 11 June 1993, in final form 8 November 1993)

ABSTRACT

In an effort to improve operational forecasts of mesoscale convective systems (MCSs), a mesoscale version of the operational Canadian Regional Finite-Element (RFE) Model with a grid size of 25 km is used to predict an intense MCS that occurred during 10–11 June 1985. The mesoscale version of the RFE model contains the Fritsch–Chappell scheme for the treatment of subgrid-scale convective processes and an explicit scheme for the treatment of grid-scale cloud water (ice) and rainwater (snow).

With higher resolution and improved condensation physics, the RFE model reproduces many detailed structures of the MCS, as compared with all available observations. In particular, the model predicts well the timing and location of the leading convective line followed by stratiform precipitation; the distribution of surface temperature and pressure perturbations (e.g., cold outflow boundaries, mesolows, mesohighs, and wake lows); and the circulation of front-to-rear flows at both upper and lower levels separated by a rear-to-front flow at midlevels.

Several sensitivity experiments are performed to examine the effects of varying initial conditions and model physics on the prediction of the squall system. It is found that both the moist convective adjustment and the Kuo schemes can reproduce the line structure of convective precipitation. However, these two schemes are unable to reproduce the internal flow structure of the squall system and the pertinent surface pressure and thermal perturbations. It is emphasized that as the grid resolution increases, reasonable treatments of both parameterized and grid-scale condensation processes are essential in obtaining realistic predictions of MCSs and associated quantitative precipitation.

1. Introduction

Due to rapid increases in computer power in recent years, operational numerical models have improved markedly by refining their numerical and physical schemes, and by increasing their grid resolution, which very soon will be high enough to resolve mesoscale convective systems (MCSs). As a consequence, growing attention is now being paid to improve mesoscale weather forecasts at numerous operational meteorological centers. These improvements have led to remarkable progress in operational prediction of large-scale pressure systems (e.g., extratropical cyclones). However, the progress in quantitative precipitation forecasts (QPFs) and severe weather warnings has lagged substantially behind the large-scale forecasts (e.g., Charba and Klein 1980; Sanders 1979). This is particularly true during the warm season when a large portion of annual precipitation is produced by MCSs (e.g., Fritsch et al. 1981; Heideman and Fritsch 1988), which are generally too small to be resolved by the conventional data network and handled by current operational models. Therefore, the improvement of the average skill in QPFs for the warm season has occurred much slower than that for the cold season (Ramage 1982). Similarly, the average skill in QPFs for precipitation systems forced by mesoscale mechanisms has been much lower than those forced by large-scale processes (Fawcett 1977; Heideman and Fritsch 1988; Fritsch and Heideman 1989). Thus, it appears that significant improvements in QPFs and severe weather warnings are possible when mesoscale weather systems can be better predicted by operational models.

Although the relationship between the grid resolution and the mesoscale structure is easy to understand, it is not clear how an increase in horizontal resolution will improve numerical prediction of mesoscale quantitative precipitation and severe weather events. First, since numerical weather prediction is an initial-value problem, the details contained in the initial conditions are of primary importance. Numerous studies have shown that numerical simulations of MCSs are very

Corresponding author address: Stéphane Bélair, Department of Atmospheric and Oceanographic Sciences, McGill University, 845 Sherbrooke Street West, Montreal, Quebec H3A 2T5, Canada.

sensitive to changes in the initial humidity, temperature, and horizontal winds (Kelly et al. 1978; Zhang and Fritsch 1986a; Chang et al. 1986). Clearly, this imposes a severe limit on the quality of mesoscale weather forecast, particularly considering that the initial conditions in an operational setting are far from adequate in providing mesoscale details. Second, as the grid resolution increases, solutions corresponding to more energetic and transient circulations may become important. Their interactions with diabatic heating/cooling and boundary-layer processes may produce significant undesirable small-scale perturbations. Thus, certain physical parameterization schemes designed for coarse-mesh models may prove inadequate for fine-mesh models. This is especially true for the treatment of moist convection that could change drastically as the horizontal grid size decreases from hundreds of kilometers to tens of kilometers (Frank 1983). For instance, the large-scale models need to parameterize both deep convection *and* mesoscale circulations, whereas mesoscale models need *only* to parameterize deep convection, since the mesoscale circulation can be explicitly resolved. As the grid size is further reduced (e.g., <5 km), all convective elements can be explicitly resolved, and convective parameterization can be bypassed. But even for a grid mesh of 10 km, some type of parameterization is still needed in order to remove rapidly conditional instability in a vertical column and help activate grid-box saturation at the right time and location (Zhang et al. 1988). Therefore, for models with intermediate grid size (i.e., 20–30 km), it is essential that a realistic convective parameterization be coupled with an explicit scheme treating solid, liquid, and vapor phases (Zhang et al. 1988; Molinari and Dudek 1992). Such an approach has proven to provide a broader spectrum of interactions between the subgrid- and the grid-scale circulation, and thus, it will also be adopted for the present study.

Using the above-mentioned approach with The Pennsylvania State University/National Center of Atmospheric Research (PSU/NCAR) Mesoscale Model (Anthes et al. 1987), in which the Fritsch–Chappell (1980, hereafter FC) convective scheme and an explicit scheme were incorporated, Zhang et al. (1989, hereafter ZGP) have obtained a successful simulation of an intense squall line that occurred on 10–11 June 1985 during Preliminary Regional Experiments for STORM-Central (PRE-STORM, Cunning 1986). For this case, the Limited-Area Fine-Mesh Model at the National Meteorological Center (NMC) and the spectral model at the Canadian Meteorological Centre (CMC) failed in predicting total precipitation and severe weather events associated with this MCS. Clearly, the coarse grid meshes used at the time in these models (for example T59 for the Canadian spectral model) could partly explain the failure. It is unlikely, however, that the squall system could be well predicted by simply increasing the horizontal resolution to 20–30 km. Therefore, a first objective of this study is to demonstrate, with the Canadian Regional Finite-Element (RFE) Model, the potential for operational models to predict the internal structure and evolution of MCSs and to significantly improve QPFs and severe weather warnings if both high grid resolution and compatible model physics are implemented. A second objective is to determine the sensitivity of the numerical prediction of the 10–11 June 1985 squall line to different implicit and explicit condensation schemes and to different sets of initial conditions.

Mesoscale versions of the RFE model have been applied in the research mode to a wide variety of wintertime meteorological events, including explosive marine cyclogenesis (Benoit et al. 1989; Mailhot et al. 1989; Mailhot and Chouinard 1989), springtime continental cyclonic development (Staniforth and Mailhot 1988), polar air mass transformation (Mailhot 1992), and polar lows (Roch et al. 1991). However, the model has not been fully tested with summertime cases in which larger-scale forcing is relatively weak and the atmosphere is less stable. Hence, the present study represents the first effort to assess more thoroughly the performance of the RFE model in predicting the internal structure and evolution of MCSs, through the case of the 10–11 June 1985 squall system.

The presentation of the results is organized as follows. Section 2 describes the mesoscale version of the RFE model. Section 3 provides verification of the control prediction against detailed observations. Section 4 presents the sensitivity of the model forecast to varying model physics and initial conditions. A summary and concluding remarks are given in the final section.

2. Model system and initialization

The mesoscale version of the RFE model used to simulate the 10–11 June 1985 MCS is very similar to the current version of the operational model. The main differences include (i) a decrease of the horizontal grid size to 25 km (as compared to 50 km in the recently implemented operational version) in the core region of the variable grid (Fig. 1), (ii) the incorporation of an explicit moisture scheme and a more appropriate convective parameterization; and (iii) the enhancement of the CMC analysis to include some mesoscale details. Table 1 summarizes the basic features of the RFE model used for this study.

a. Dynamics

Staniforth and Daley (1979) and Tanguay et al. (1989) provide a detailed description of the dynamical and numerical aspects of the RFE model. The hydrostatic primitive equations in σ coordinates (pressure normalized by surface pressure) are integrated using a semi-implicit temporal discretization and a finite-element spatial discretization. The finite-element tech-

TABLE 1. Summary of the mesoscale RFE model.

Numerics
- 3D hydrostatic primitive equations
- semi-implicit time discretization
- semi-Lagrangian scheme for 3D advection (time step: 300 s)
- linear finite elements in (x, y, σ)
- variable horizontal resolution grid overlaid on a polar stereographic projection (25 km in fine grid)
- 19 σ levels with high resolution in the lowest 150 mb
- second-order horizontal diffusion for temperature, vorticity, and divergence
- 0.5° orography field

Physics
- planetary boundary layer (PBL) based on turbulent kinetic energy
- diagnostic PBL height
- implicit vertical diffusion
- surface energy budget based on force–restore method
- diurnal cycle with solar and infrared fluxes at ground modulated by clouds
- infrared and solar radiation fluxes calculated at all levels
- diagnostic cloud cover
- Fritsch–Chappell scheme for parameterized moist convection
- explicit moisture scheme containing prognostic equations for cloud water/ice and rainwater/snow

nique provides the flexibility to use a uniform, high-resolution mesh in the central domain surrounded by a smoothly varying resolution mesh in which the grid size increases by a constant factor until the equator is reached (Fig. 1). This variable resolution self-nesting strategy is quite useful for regional-scale and mesoscale modeling (Staniforth and Mitchell 1978; Staniforth and Mailhot 1988) and has several advantages (Gravel and Staniforth 1992). Solid wall flow conditions are imposed at the lateral boundaries tangent to the equator. A semi-Lagrangian scheme is used to treat horizontal and vertical advection, which allows a much longer time step (with no loss of accuracy) than Eulerian-based advection schemes whose time step is limited by numerical stability. Here, a time step of 300 s is used for the present model integration with a fine-mesh size of 25 km.

b. Physics

The RFE model contains a comprehensive set, with several options, of parameterization schemes of physical processes (Benoit et al. 1989; Mailhot et al. 1989). In the present study, several important additions and improvements to the physics have been incorporated in order to better address the numerical prediction of summertime MCSs and severe weather events. In particular, a detailed convective parameterization scheme including moist downdrafts and an explicit microphysical scheme have been added. The basic properties of these two schemes are described briefly herein.

In the mesoscale version of the RFE model, an improved version of the Fritsch and Chappell (1980) convective parameterization scheme has been incorporated (Zhang and Fritsch 1986b). In this scheme, the convective available potential energy (CAPE) determines the amount of convective heating, moistening, and precipitation, and it is removed during a convective time scale τ_c (time needed for midlevel winds to advect horizontally the parameterized clouds across one grid length; in the scheme, this parameter is forced to lie between 30 and 60 min). The scheme divides a grid box into three parts: convective updrafts, moist downdrafts, and compensating subsidence. It is assumed that convective effects are dominated by deep clouds; thus, this scheme is most suitable for a grid length of about 20–25 km. Deep convection is triggered when the mixed boundary-layer air is warmer than its environment after it is raised to the lifting condensation level and warmed by a temperature perturbation being proportional to $w^{1/3}$, where w is the grid-scale vertical velocity. The air parcel accelerates upward as long as it is buoyant; it entrains environmental air while moving upward and detrains condensate after reaching the equilibrium level. Moist downdrafts behave in a way similar to updrafts, except that they are initiated at the level of free sink, which is often the level with the minimum equivalent potential temperature (see Fritsch and Chappell 1980). The inclusion of moist downdrafts has been shown to be essential in reproducing many important meso-β-scale structures of MCSs, particularly for those that occurred within weak gradient environments (Zhang and Fritsch 1988; Zhang and Gao 1989).

The resolvable-scale moist physics scheme used follows that described in Hsie et al. (1984), Zhang (1989), and Dudhia (1989). This scheme treats cloud water (ice) and rainwater (snow) as prognostic variables. Thus, two additional equations are solved and the equations for specific humidity and temperature are modified to account for the effects of all diabatic processes. They include (i) virtual temperature in the ideal gas law, (ii) water loading in the hydrostatic equation, (iii) condensation/evaporation, freezing/melting, and sublimation/deposition of condensate, (iv) autoconversion and accretion of cloud water/ice into rainwater/snow, and (v) fallout of rainwater/snow. A simple and economic strategy is adopted to treat cloud water/ice and rainwater/snow, in which the solid phases are allowed to exist at levels with temperature less than 0°C and the liquid phases (i.e., cloud water and rainwater) at temperature above 0°C.

c. Initialization procedures

As in other national centers (e.g., Mills and Seaman 1990; DiMego et al. 1992), CMC has recently implemented a regional data assimilation spinup cycle to replace the previous global analysis system for initializing the RFE model (Chouinard et al. 1994). Apart from providing higher-resolution initial conditions, this

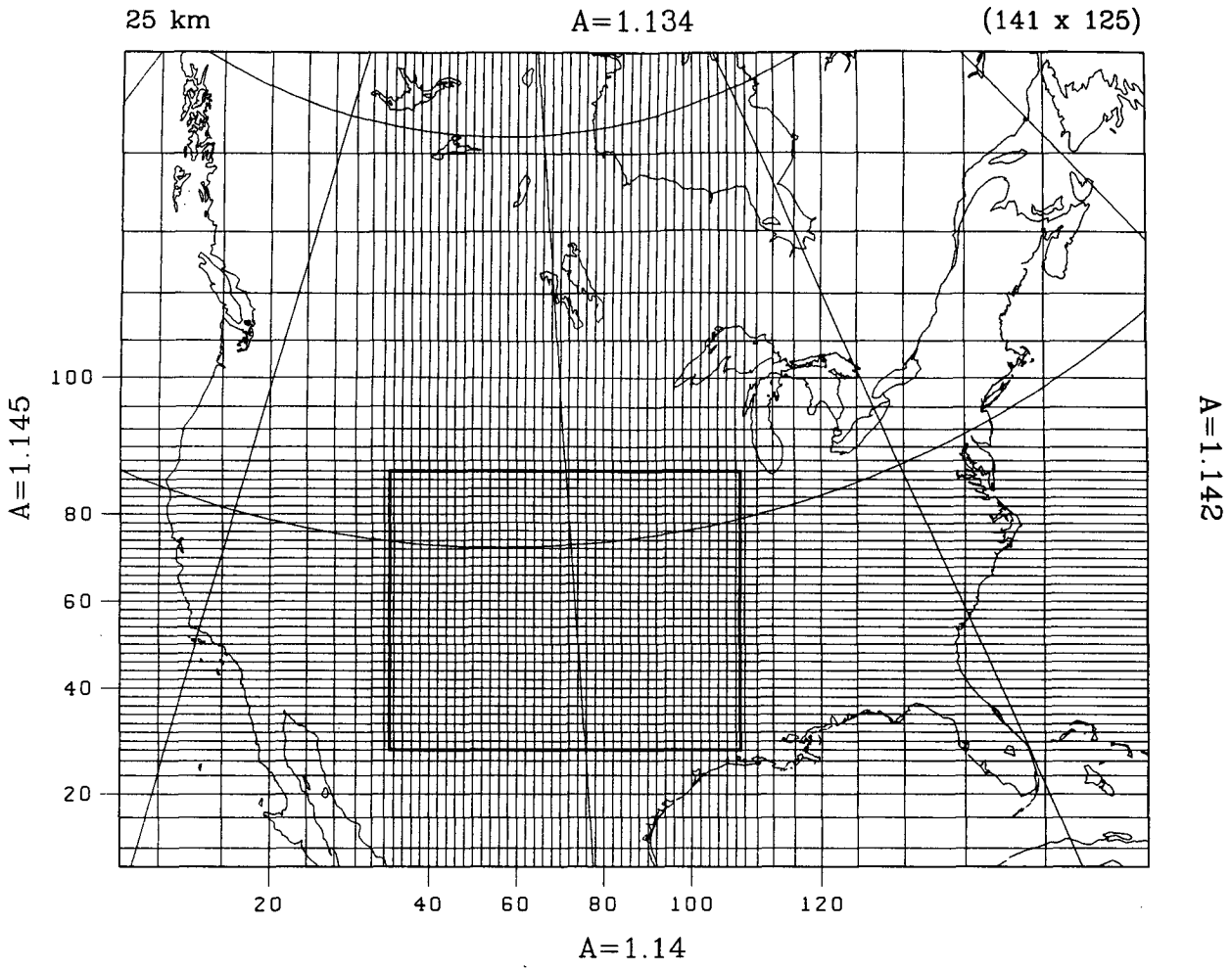

FIG. 1. Portion of the 141 × 125 hemispheric variable grid mesh projected on a polar stereographic plane. The heavy rectangle indicates uniform high resolution of 25 km with the grid size increasing by the constant factors 1.134 northward, 1.142 eastward, 1.140 southward, and 1.145 westward.

assimilation system provides dynamically balanced fields to reduce initial moisture and precipitation spinup problems. However, this regional analysis system was not readily available for the present study, so a simple procedure, described in the following, was adopted to obtain better initial conditions. The RFE model is initialized at 1200 UTC 10 June 1985 with a blend of initial conditions from the CMC archived analysis and the limited-area PSU/NCAR analysis used by ZGP. Specifically, the initialization procedure begins by interpolating the archived CMC objective analysis from low resolution (the resolution was around 300 km at that time) to the variable resolution grid mesh. To add mesoscale details to the CMC analysis, the initial conditions used by ZGP are employed to enhance the analysis over a limited area covering most of North America. The ZGP initial conditions are obtained using the PSU/NCAR analysis package. This analysis essentially uses the NMC global analysis as first-guess fields, which are enhanced with the standard rawinsonde observations over North America using a Cressman-type objective analysis technique (Benjamin and Seaman 1985). The high-resolution fields resulting from this analysis over a limited area are then incorporated into the CMC analysis by a Cressman (1959) analysis and will be referred to as the enhanced analysis (to contrast with the original CMC analysis). No balancing between mass and wind field is done; only the vertically integrated divergence is removed from the wind fields to minimize the noise early in the model integration. No further initialization procedure is performed for the present study. Note that only conventional data are used in the procedures described above, since the PRESTORM network did not collect supplementary data until 2100 UTC 10 June when the squall line developed and began to move into the network.

3. Model verification

Figure 2 shows larger-scale conditions at the surface and 700 mb at the model initial time (i.e., 1200 UTC 10 June 1985). A southwest–northeast-oriented shallow surface cold front and a midlevel short-wave trough were located in the western part of Colorado. Later, they moved southeast toward the PRE-STORM network and provided an important triggering mechanism for the development of the squall line. A weak surface cyclonic vortex was present near the intersection of Wyoming, Nebraska, and South Dakota. Worthy of notice is the presence of a decaying MCS that was responsible for high relative humidity over the network region at the model initial time. A low-level jet brought warm and moist air over Texas into the PRE-STORM network.

Figure 3 compares the model-predicted sea level pressure, surface temperature, and accumulated rainfall distribution to the mesoscale analysis by Johnson and Hamilton (1988, hereafter referred to as JH). The JH analysis shows that the squall line was initiated around 2100 UTC 10 June ahead of the surface cold front. Then, the squall line intensified rapidly as it propagated southeastward into the network. At 0000 UTC (Fig. 3a), the squall gust front intersected a weak outflow boundary associated with the decaying MCS in eastern Kansas. The squall system entered its mature stage at 0300 UTC (Fig. 3b). Its surface pressure distribution is characterized by a presquall mesolow, a mesohigh, and a wake low. By 0600 UTC, the squall line began to dissipate as it was about to move out of the network (Fig. 3c). A mesohigh and two wake lows were quite evident in the JH analysis. The passage of the squall system during its life cycle has also been well captured by rawinsondes, conventional and Doppler radars, and wind profilers (see JH; Rutledge et al. 1988; Biggerstaff and Houze 1991a,b).

Although the RFE model was initialized with conventional observations, it reproduces very well many observed mesoscale details of the event. First, the model predicts reasonably the initiation of the squall line at nearly the right time and location, and it also captures the dissipating MCS over eastern Kansas and Oklahoma during the initial hours (not shown). At 0000 UTC (Fig. 3d), the predicted squall position and the outflow boundary associated with the decaying MCS conform reasonably well to that observed. Second, as the system moves southeastward and enters the mature stage, the model reproduces the presquall mesolow, mesohighs, and wake lows (Figs. 3e, f). The orientation and propagation of the squall line also compares favorably to the JH analysis. Third, the RFE model predicts a temperature gradient of about 6°C across the squall line, which agrees with the 5°–8°C values analyzed by JH. Note that the arc-shaped portion of the squall line is also well depicted by the forecast. These results are very encouraging, particularly when considering that all these meso-β-scale features are generated from initial conditions using only conventional data. The results suggest that the boundary layer, the convective parameterization scheme, and the explicit moisture physics used in the model are realistic enough to reproduce the evolution of the squall system.

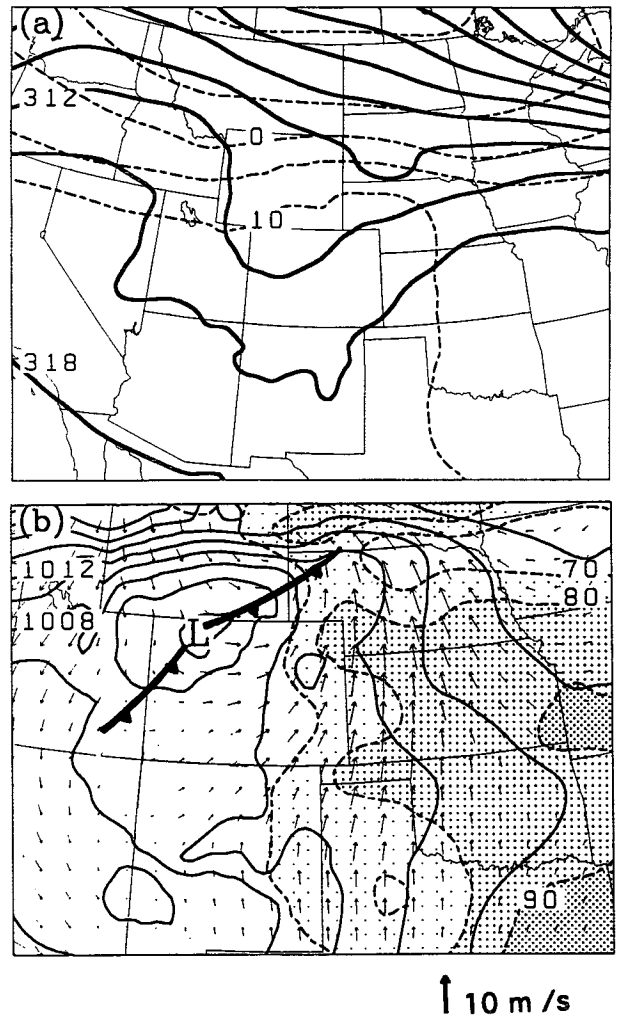

FIG. 2. Enhanced initial conditions at 1200 UTC 10 June 1985. (a) 700-mb geopotential height (solid, every 3 dam) and temperature (dashed, every 5°C); (b) surface relative humidity (dashed, every 10%), surface wind vectors, and sea level pressure (solid, every 2 mb). Different shadings are used to indicate values of relative humidity greater than 70%, 80%, and 90%.

The realistic prediction of the squall system is further evidenced by the evolution of resolvable-scale and parameterized rainfall rates (see Figs. 3g–i). The distribution and orientation resemble the radar reflectivity analysis (Fig. 4) by Rutledge et al. (1988) and the composite radar reflectivity constructed by Biggerstaff and Houze (1991a). Specifically, the model handles reasonably well two different types of precipitation mechanisms, namely, a line of (parameterized or implicit) convective precipitation that is trailed by a zone

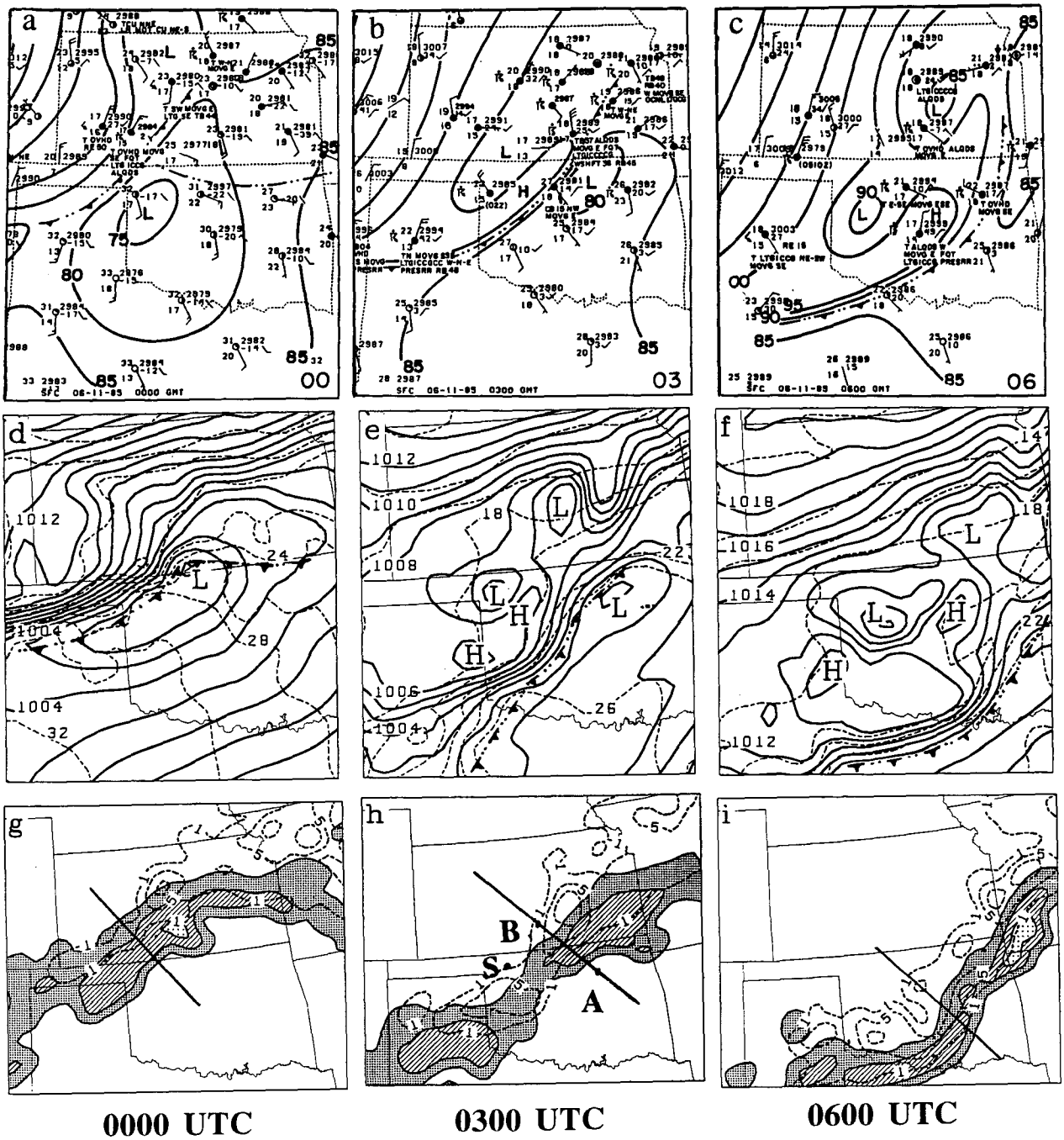

FIG. 3. The upper panel shows surface mesoanalyses from Johnson and Hamilton (1988) at (a) 0000 UTC, (b) 0300 UTC, and (c) 0600 UTC 11 June 1985. Dashed double-dot lines indicate outflow boundaries. Pressures are converted to 518 m: units are in Hg—for example, 85 = 29.85 in Hg (note that 1 in Hg = 33.9 mb). Wind speeds are denoted with a full barb equal to 5 m s^{-1}. The middle panel shows the predicted sea level pressure (solid, every 1 mb) and surface temperature (dashed, every 2°C) from (d) 12-h, (e) 15-h, and (f) 18-h control integration. The lower panel shows the predicted grid-scale (dashed) and convective (shaded) rainfall rates with contours denoting 1, 5, 10, and 20 mm h^{-1} valid at (g) 0000, (h) 0300, and (i) 0600 UTC 11 June 1985. The predicted sounding at point S is given in Fig. 7, and vertical profiles of θ_e ahead and behind the line (points A and B) are shown in Fig. 10.

of (resolvable or explicit) stratiform precipitation. The magnitude of the stratiform precipitation increases with time and reaches its maximum extent near 0600 UTC. It is interesting to note that the model produces one convective rainfall maximum to the south and another one to the north along the leading line during the ma-

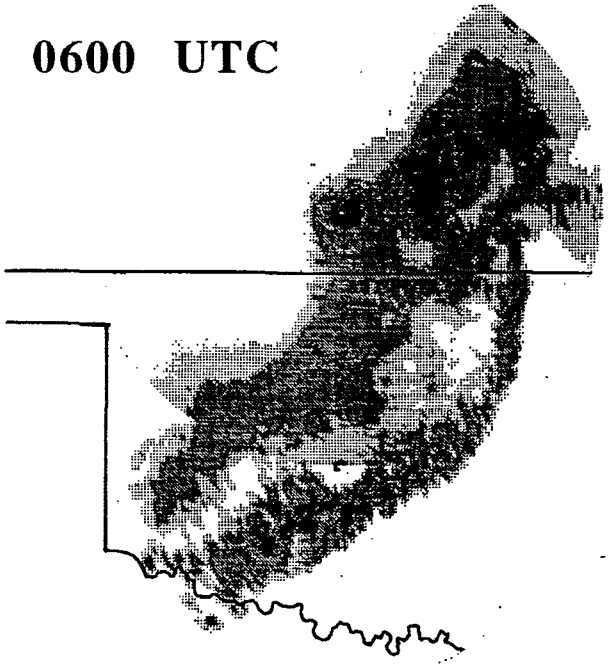

FIG. 4. Radar reflectivity analysis at 0600 UTC 11 June 1985 (from Rutledge et al. 1988).

ture and decaying stages, with two corresponding rainfall maxima in the trailing stratiform region. Between these two types of rainfall maxima there is a zone of weaker precipitation called the "transition zone" (Smull and Houze 1985). According to Biggerstaff and Houze (1991a), the enhanced stratiform precipitation resulted from a cooperative process in which precipitation-sized particles are supplied by the convective portions ahead and increased by condensation/depositional growth in the strong mesoscale ascent (see their Fig. 15).

Figure 5 compares the predicted accumulation of precipitation to the JH analysis. In general, the distribution and amount compare favorably with that observed. For example, the model predicts a maximum of more than 60 mm of total precipitation in the northern part of the PRE-STORM network, of which the implicit (or FC) scheme accounts for 60% of the total production. The explicit scheme also produces a significant fraction of precipitation associated with the squall system, with two maxima located near the major wake lows. Note that the predicted grid-scale precipitation is larger than the analyzed. This appears to be due to the use of different procedures to partition total precipitation into convective and stratiform components. The observational analysis of precipitation in JH is based on the magnitude of relative rainfall rates (i.e., a rainfall rate of <5 mm h^{-1} is defined as "stratiform"; otherwise defined as "convective"), whereas the modeled grid-scale precipitation is generated by grid-box (25 km $\times$ 25 km) saturation, in which some portion could be treated as "convective." Therefore, the predicted stratiform rainfall accounts for roughly 45% of the total accumulations, as compared to 29% analyzed by JH.

Of further importance for this integration is the model's capability to predict other important meso-β-scale elements (see Fig. 6). Specifically, it is encouraging that the model reproduces remarkably well an overturning updraft along the leading line, a front-to-rear (FTR) ascending flow extending from the boundary layer ahead of the system to the trailing stratiform region near the tropopause, and a rear-to-front (RTF) descending flow beneath the stratiform clouds. Note how the area of grid-box saturation and precipitable water content expands rearward as the system evolves. By 0600 UTC, a stratiform region of 300 km in width has formed behind the convective line, with the corresponding internal circulations tilting upshear. This upshear tilt is a typical characteristic of squall systems at the decaying stage (Rotunno et al. 1988). Zhang and Gao (1989) have demonstrated that these circulation structures can be realistically reproduced mainly because of the use of a coupled explicit-convective parameterization package that includes the effects of moist downdrafts. This point will be further shown in the next section. Specifically, with an explicit moisture scheme, condensate is generated in and allowed to move with the FTR ascending flow. As condensate falls into a subsaturated column, grid-scale downdrafts could be induced by cooling from sublimation, melting, and evaporation. As a result of the latent heating and cooling occurring at different locations, various internal structures of the squall system can be induced. In the present case, whether or not the RTF descending flow can be well generated determines the development of other meso-β-scale elements within the squall system (Zhang and Gao 1989; Zhang 1992). As shown in Fig. 6b, the descending flow is most intense along the interface between the leading edge of a dry pocket and the stratiform cloud boundary, thus corresponding to more pronounced cooling by sublimation, melting, and evaporation. Toward the rear, less precipitable water is available for evaporation, so adiabatic warming exceeds diabatic cooling, which gives rise to an onion-shaped sounding near the center of a wake low (see Fig. 7). This process is also responsible for the generation of surface wake lows (see discussions in JH and ZGP). The role of cold outflow (Figs. 3d–f) in helping to trigger new convection ahead of the leading line is also evident from Fig. 6b.

4. Sensitivity experiments

After documenting in the preceding section the remarkable agreement between the predicted and the observed events, it is now possible to use that forecast as a control run to assess the relative importance of various processes in obtaining the successful prediction.

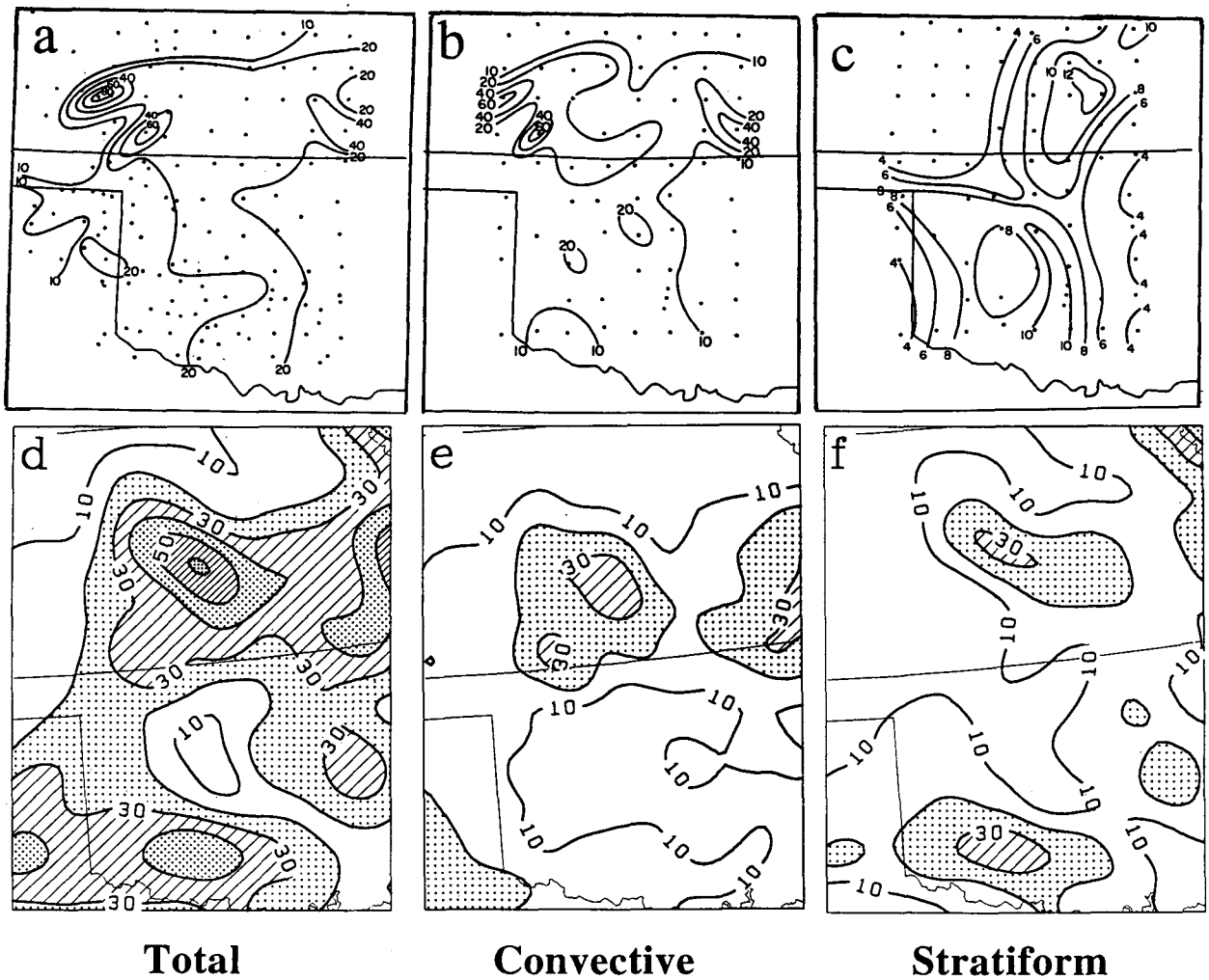

FIG. 5. The upper panel shows the observed accumulated rainfall amount (every 10 mm) analyzed for (a) entire squall system, (b) convective portion, and (c) stratiform portion (from Johnson and Hamilton 1988). The lower panel shows the predicted rainfall amount (every 10 mm) between 2100 UTC 10 June and 1200 UTC 11 June 1985 for (d) total precipitation, (e) convective portion, and (f) grid-scale portion.

This can be done by determining the sensitivity of the model solution to changes in certain parameters while holding all other parameters identical to those in the control run. Four sensitivity experiments are conducted to test the effects of different parameterization schemes for condensation and the impact of the initial conditions (see Table 2). The impacts of evaporation, ice microphysics, parameterized moist downdrafts, and water loading have been investigated by Zhang and Gao (1989), and the effects of using the Arakawa-Schubert (1974) convective scheme has been tested by Grell (1993), both with the PSU/NCAR Mesoscale Model.

a. The moist convective adjustment scheme (MCA)

Due to its attractive simplicity, the moist convective adjustment (MCA) scheme introduced by Manabe et al. (1965) to handle convective precipitation has been widely used in large-scale models (e.g., Kurihara 1973; Krishnamurti et al. 1980) and, until recently, in the operational RFE model. In this scheme, vertical adjustment of temperature and moisture takes place only for the part of the sounding for which the relative humidity and the lapse rate exceeds 90% and the moist adiabatic lapse rate, respectively. Thus, the purpose of this experiment is to examine the performance of the RFE model in predicting the 10–11 June 1985 squall events when the FC implicit scheme is replaced by an MCA-type scheme.

Despite the simplicity of the MCA scheme, the model reproduces a line of intense precipitation that propagates southeastward across the network (see Fig. 8). However, there are several deficiencies with the integration. First, the squall line is initiated around

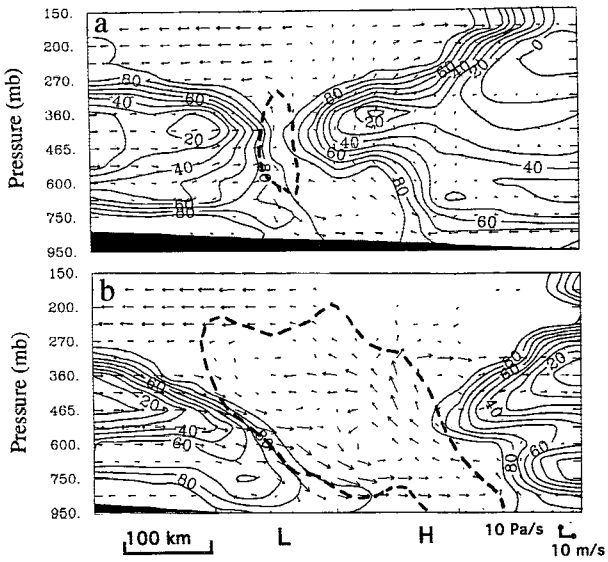

FIG. 6. Vertical cross section of relative humidity (solid lines, every 10%) and precipitable water boundaries (>1 g kg^{-1}, dashed lines), superposed with relative flow vectors normal to the squall line at (a) 0000 UTC and (b) 0600 UTC 11 June 1985. The cross sections are taken along lines given in Figs. 3g,i.

0000 UTC 11 June, which is 3 h later than that in the control run. This delay appears to be related to the initial model spinup problem in which a critical relative humidity value has to be reached before allowing vertical adjustment, whereas in the control run the activation of the FC scheme does not require such a condition to be met. This 3-h delay also accounts for the lag of the predicted squall system in the MCA run. Second, the squall system displays an east–west orientation, as compared to the actual northeast–southwest orientation of the system (cf. Figs. 4 and 8). This could also be attributed to the basic assumption involved in the MCA scheme. Specifically, because of the relatively moist atmosphere over central and eastern Kansas, the convective adjustment and the associated forcing take place earlier than that to the west. This can be seen from the more extensive parameterized and explicit rainfall over the region (see Fig. 8a). Third, the MCA integration produces a wider convective region and a more extensive area of stratiform rainfall, as compared to the control run. In particular, a large area of these two rainfall regimes is overlapped, indicating that much of the explicit heating occurs under convectively unstable conditions. As a result, strong upward motion (>1 m s^{-1}) has developed in the convective region (not shown).

Figure 9 shows the distribution of sea level pressure and surface temperature from 18-h prediction using the MCA scheme. Clearly, the scheme could produce low-level cooling in the lower layers that leads to the generation of strong temperature and pressure gradients across the squall system. However, the model when using the MCA fails to reproduce the mesohighs associated with cold downdrafts (parameterized and resolvable-scale) and wake lows associated with descending rear inflow, even though a significant amount of precipitable water is available behind the convective line. This appears to be attributable to the lack of strong grid-scale cooling. In particular, as suggested by the extensive area of explicit precipitation given in Figs. 8a–c, the atmosphere behind the convective region is saturated throughout the troposphere (not shown), so very weak grid-scale sublimation and evaporation occur. Zhang and Gao (1989) showed that the grid-scale cooling is instrumental in generating the intense descending rear inflow and surface pressure perturbations.

To gain further insight into the role of different convective schemes in stabilizing a vertical column, Fig. 10 displays vertical profiles of equivalent potential temperature (θ_e) that are taken ahead of and behind the squall system. It is obvious that the FC scheme removes efficiently almost all of the CAPE by heating/moistening the upper troposphere and cooling/drying the lower troposphere. In contrast, the MCA scheme produces a deep layer of substantial cooling and drying in the lower half-portion of the atmosphere, but it hardly affects the θ_e profile aloft. Apparently, this is because the vertical adjustment scheme acts only locally and it could not penetrate into the potentially stable layers in the upper troposphere. As a result, the vertical stabilization is not as complete as that in the control run.

b. *The Kuo scheme (KUO)*

The RFE model physics contains, as an option, the Kuo (1974) cumulus parameterization scheme (see Mailhot et al. 1989) that includes a simplified description of microphysical processes, such as evaporation of precipitation, formation of liquid/solid precipitation, and freezing/melting of precipitation phases. The Kuo scheme is activated when the column-integrated

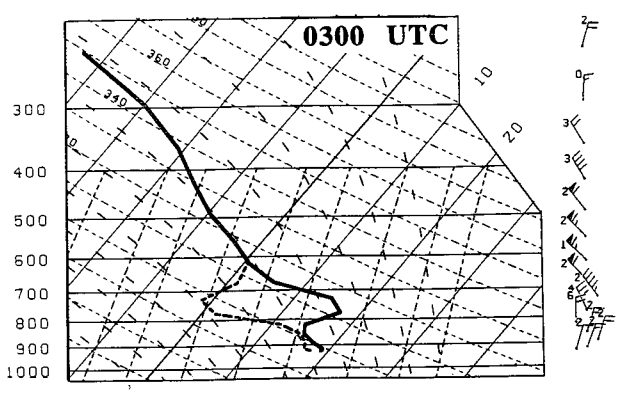

FIG. 7. Predicted sounding near the center of the southern wake low, valid at 0300 UTC 11 June 1985. (See point S in Fig. 3h for the location.)

TABLE 2. Experimental design.

Experiment	Implicit scheme	Explicit scheme	Initial conditions
CONTROL	Fritsch–Chappell	Explicit moisture scheme	Enhanced analysis
MCA	Moist convective adjustment	Explicit moisture scheme	Enhanced analysis
KUO	Kuo	Explicit moisture scheme	Enhanced analysis
SES	Fritsch–Chappell	Simple supersaturation removal	Enhanced analysis
CMC	Fritsch–Chappell	Explicit moisture scheme	CMC analysis

moisture convergence exceeds a critical value and the sounding becomes conditionally unstable. Then a fraction (b) of total moisture convergence is stored and acts to increase the humidity of the column while the remaining fraction ($1 - b$) is condensed and precipitated. Since the Kuo type of convective scheme has been widely used for meso-α-scale or larger-scale simulations of extratropical cyclones, polar lows and MCSs, and also for a number of operational models (e.g., in the Nested-Grid Model at NMC and in the current 50-km version of the operational RFE model at CMC), the purpose of this experiment is to determine if it is capable of reproducing the observed meso-β-scale structures as well as quantitative precipitation associated with the 10–11 June 1985 squall line.

Unlike that with the MCA scheme, the model with the Kuo and explicit moisture schemes is able to initiate the squall line at nearly the right time and location (see Fig. 11). When a grid size of 50 km is used, however, the squall line is not initiated until 0000 UTC (not shown). This 3-h delay is a typical spinup problem associated with coarse-resolution models. Thus, the right timing and location in the current run indicate that the 25-km grid size is appropriate for examining the effects of various model physical processes on the subsequent evolution of the squall system.

While the RFE model with the Kuo scheme predicts reasonably the incipient stage of the squall system, it cannot cause the system to propagate as fast as the observed and the control run. By 0600 UTC, the simulated squall line lags at least 150 km behind. This slowness is again attributable to the lack of cold downdrafts in the Kuo scheme, since downdrafts are important dynamics in the movement of squall lines. Of further significance is that grid-scale precipitation is almost absent throughout the 18-h integration. Obviously, there are two possible reasons for this problem: (i) the convectively induced vertical circulation may be too weak to bring enough moisture upward for triggering grid-box saturation, or (ii) the Kuo scheme may remove too much moisture in a vertical column (i.e., a small "b" parameter), especially in the lower layers. The first possibility is not likely the case after comparing Figs. 3 and 11, for the Kuo scheme run produces greater convective precipitation rates along the leading line during the formative stage than that with the FC scheme. The maximum rainfall rates, generated to the north of the leading line, are of the order of 30 mm h^{-1}, which is equivalent to an average heating rate of 7.5°C h^{-1} throughout a vertical column. A comparison of the vertical θ_e profiles ahead of and behind the convective line indicates that the second possibility is most likely the case. Specifically, Fig. 10 shows that the Kuo scheme reduces substantially the magnitude of θ_e in the lower troposphere after the passage of the line, with little change occurring higher up. This reduction is mainly caused by a decrease in moisture content, since the Kuo scheme does not contain the cooling effect associated with moist downdrafts (also see Fig. 12). On average, the "b" parameter is of the order of 5%–15%. The greatest reduction of θ_e occurs in the lowest layer where ample moisture is stored. This suggests that

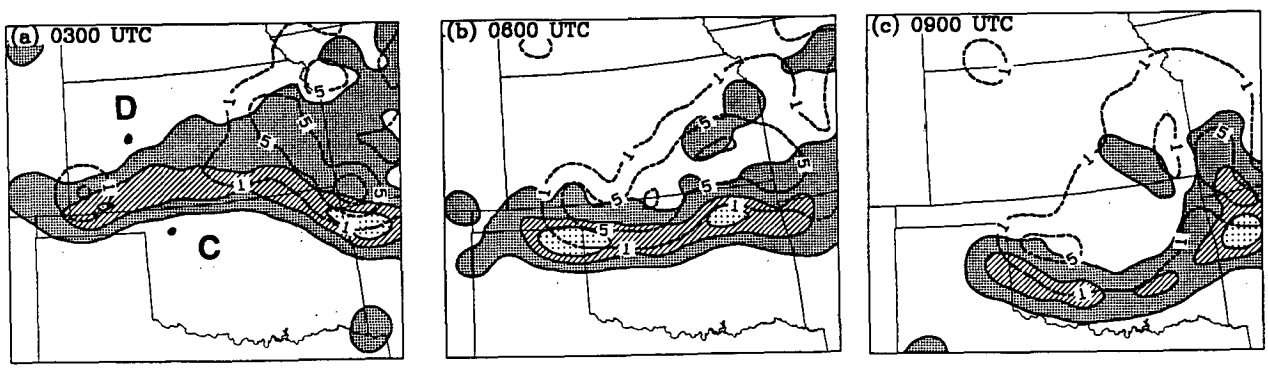

FIG. 8. As in Figs. 3g–i but for experiment MCA (moist convective adjustment). The letters "C" and "D" denote the locations of θ_e profiles shown in Fig. 10.

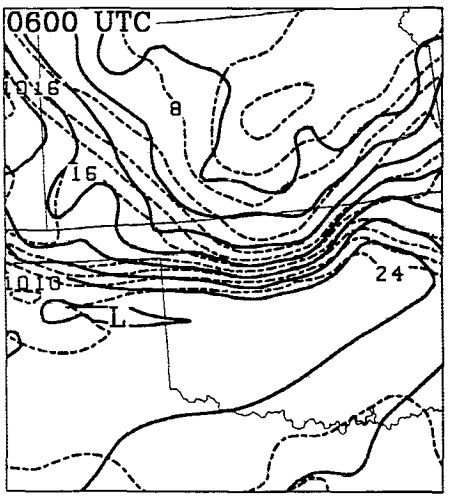

FIG. 9. As in Fig. 3f but for experiment MCA (moist convective adjustment). Note that the isobars are drawn every 2 mb.

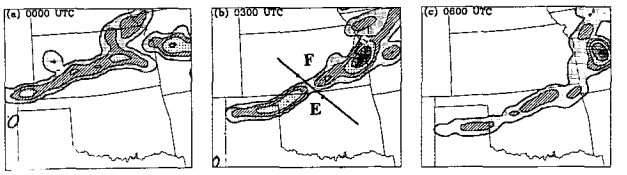

FIG. 11. As in Figs. 3g–i but for experiment KUO. The letters "E" and "F" denote the locations of θ_e profiles shown in Fig. 10.

the convective drying could be excessive in the boundary layer, so the grid-box saturation and grid-scale latent heat release are significantly delayed (Zhang et al. 1988). In the present case, this delay is further aggravated due to the absence of strong larger-scale forcing. By comparison, the FC scheme produces a marginally stable θ_e profile within a deep layer, although it has also removed a similar amount of θ_e in the lowest layer. However, the removed amount of θ_e by the FC scheme results from a combination of cooling and drying associated with moist downdrafts.

Because of the lack of downdraft cooling in the Kuo scheme and because of the negligible effect of grid-scale latent heat release in the present run, the model fails to produce significant surface pressure perturbations, such as mesohighs, wake lows, and cold outflow boundaries (Fig. 12). The elongated pressure trough ahead of the convective line is just a part of the surface frontal system; it can be traced back to the low pressure zone at the model initial time (see Fig. 2b). Similarly, without the downdraft cooling, the model is unable to reproduce the basic internal circulations of the squall system, as shown in Fig. 13b. Apparently, the rear inflow stays elevated as a consequence of little condensate available for evaporation. A well-organized FTR ascending flow does not develop, because the Kuo scheme fails to induce strong mass perturbations in the midtroposphere and upper troposphere, as can also be seen from Fig. 10. The less significant role of the grid-scale latent heat release is also part of the reason. The results suggest that the Kuo scheme may be only suitable for predicting the timing and location of convective initiation, or the incipient organization of MCSs, but not appropriate for predicting the associated precipitation systems at the mature stage. In contrast, in the control run, the FC scheme tends to efficiently stabilize potentially unstable columns along the leading line and leave behind nearly saturated conditions, and then the explicit scheme takes over to generate latent heating in

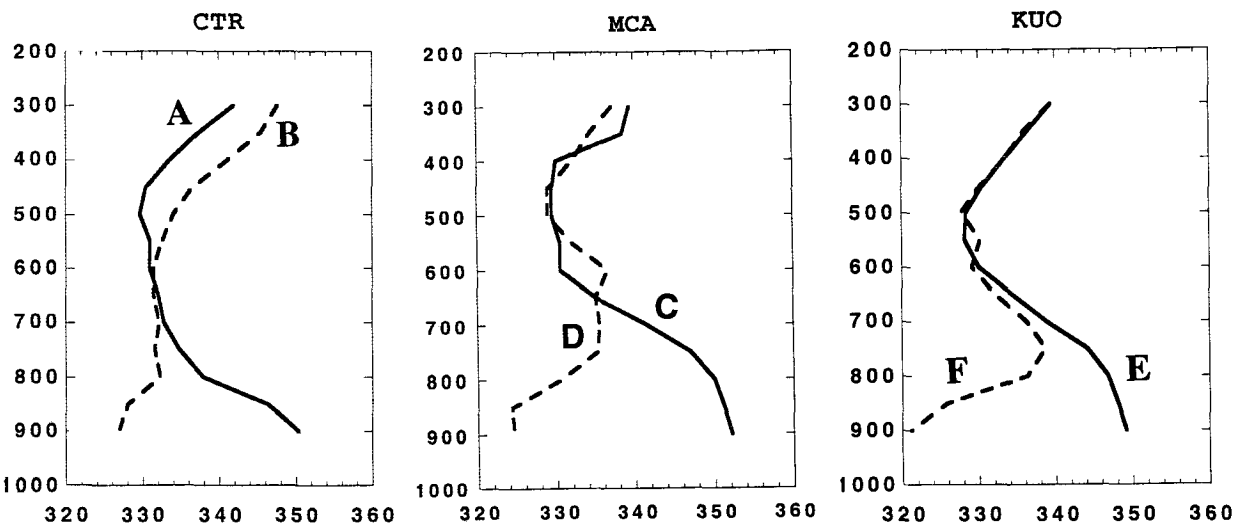

FIG. 10. Predicted equivalent potential temperature (θ_e) profiles taken ahead of and behind the leading convective line from 15-h integrations for (a) control run (see Fig. 3h for the locations), (b) experiment MCA (see Fig. 8a), and (c) experiment KUO (see Fig. 11b).

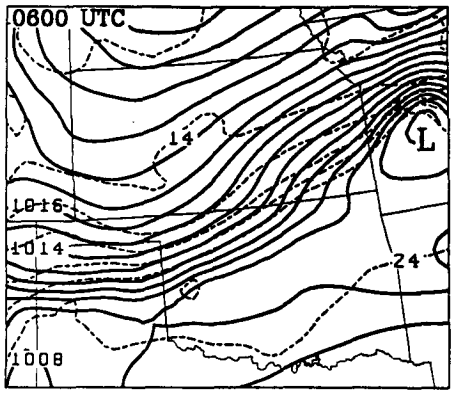

FIG. 12. As in Fig. 3f but for experiment KUO.

the FTR ascending flow and diabatic cooling in the RTF descending flow, thereby leading to the development of a well-organized slantwise circulation in the stratiform region. Such a slantwise circulation is instrumental in the production of stratiform precipitation, based on the analysis of moist potential vorticity by Zhang and Cho (1992).

c. *Simple explicit scheme (SES)*

After examining the model's sensitivity to different convective parameterization schemes, it is natural to evaluate the effect of the explicit moisture scheme, since Zhang et al. (1988) and Molinari and Dudek (1992) have emphasized the importance of coupling the parameterized with explicit convective processes in simulating the internal structure and evolution of MCSs. For this purpose, the prognostic explicit moisture scheme in the control run is replaced by the simple grid-box supersaturation removal scheme described in Mailhot et al. (1989), while subgrid-scale convective processes are still represented with the FC scheme.

It is apparent from Figs. 14 and 15 that use of the simple supersaturation removal scheme produces much less significant changes on the simulation of surface features, as compared to those with different convective parameterization schemes. For example, the orientation and propagation of the leading convection, as well as convective rainfall, are only slightly affected (cf. Figs. 3, 14, and 15), since they are mainly determined by parameterized moist downdrafts. More notable differences appear to the rear of the system. Specifically, the mesohighs and wake lows are significantly weaker and the extent of convectively generated pressure disturbances is much smaller than those in the control run. Because condensate is not allowed to move around, localized grid-scale precipitation develops over some regions. It is interesting that the model still produces reasonably the distribution of grid-scale precipitation that lags behind the parameterized convective precipitation, although the trailing stratiform region is relatively narrower. This phase lag appears to be determined by the squall's internal circulations. Obviously, the development of trailing grid-scale precipitation requires the presence of an FTR ascending flow that can generate and transport a sufficient amount of saturated air mass rearward (Zhang and Cho 1992). Momentum budgets by Gao et al. (1990) indicate that this type of FTR flow develops as a result of convectively generated mesohigh pressures aloft along the leading line, which are in turn determined by the convective heating and moistening. This process also helps explain why the Kuo scheme fails to induce the FTR flow, since it produces little changes of θ_e in the upper levels (cf. Figs. 10a,c).

While use of the supersaturation removal scheme only minimally affects the distribution and amount of surface precipitation, it has important dynamic impacts on the organization of the squall line's internal circulation. In particular, the lack of sublimative melting and evaporative cooling as well as condensate advection, owing to the instantaneous removal of conden-

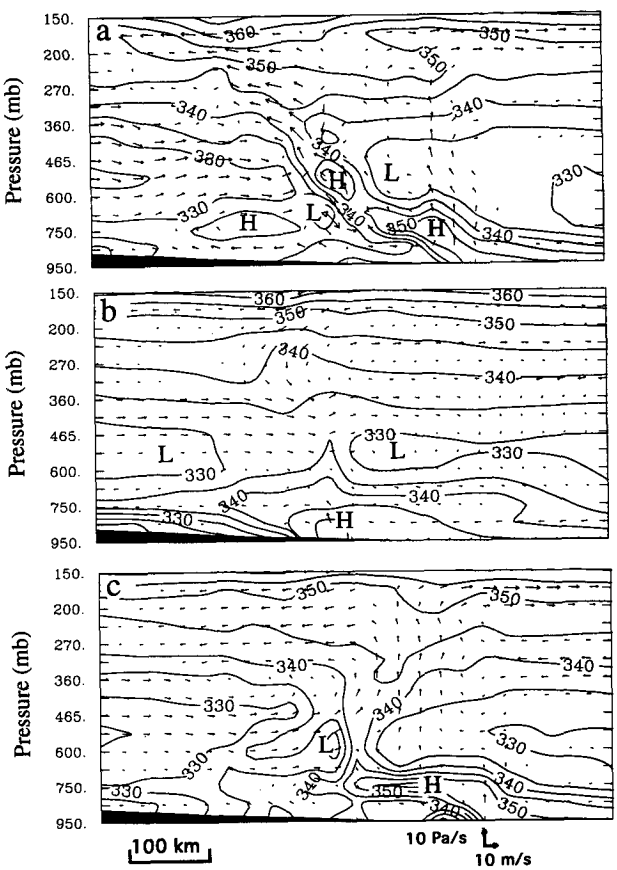

FIG. 13. Vertical cross sections of equivalent potential temperature (θ_e, every 5 K) superposed with relative flow vectors normal to the squall line from 15-h integration for (a) control run (see Fig. 3h for the location), (b) KUO (see Fig. 11b), and (c) SES (see Fig. 14b). The H's and L's refer to the thermal maxima and minima.

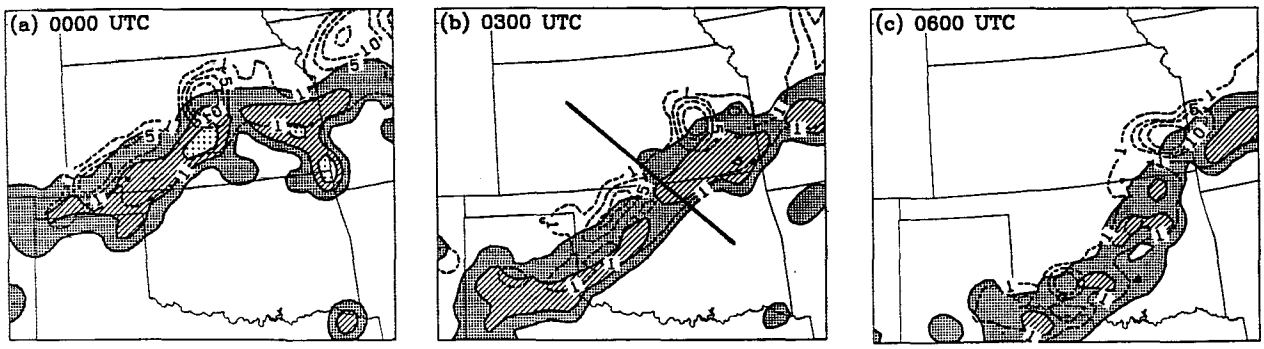

FIG. 14. As in Figs. 3g–i but for experiment SES.

sate, causes the RTF flow to stay elevated. The absence of strong descending rear inflow then leads to the generation of weak wake lows and a less evident arc-shaped structure of the leading line (cf. Figs. 3 and 14). Furthermore, a slantwise FTR ascending flow, present in the control run, never develops in the SES simulation (Weisman 1992). In the present case, horizontal vorticity associated with the FTR inflow appears to be balanced by that of the RTF inflow such that the updrafts along the leading line remain erect during most of the system's life cycle (cf. Figs. 13a,c). Overall, the squall line's circulation is much weaker than that in the control run. Since the vertical thermal structures along the leading line are nearly identical between the control run and experiment SES, the absence of the sloping flow limits the rearward transport of high-θ_e air from the boundary layer, which is crucial in the generation of trailing stratiform precipitation.

d. No enhanced analysis (CMC)

Due to the low resolution of the CMC analysis scheme used in 1985 (i.e., ~300 km), the initial conditions tend to miss certain important mesoscale details, particularly those that may be marginally resolved. For the present case, the CMC analysis produces a much weaker short-wave trough in the midtroposphere (Fig. 16a), a stronger northerly flow behind the surface front, and a slightly drier southerly flow over the PRESTORM network, as compared to the enhanced analysis used for the control run. In addition, the location and orientation of the surface front as well as the rotational flow structure differ substantially from those in the high-resolution surface observations (cf. Figs. 2b and 16b). Thus, the purpose of this experiment is to examine the sensitivity of the predicted squall system to the use of different initial conditions. In particular, we wish to see how the intensity of the midlevel short wave and the distribution of the surface frontal system would affect the organization of the squall system.

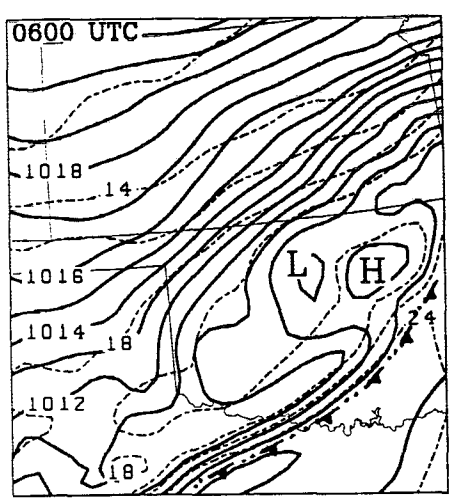

FIG. 15. As in Fig. 3f but for experiment SES.

With the CMC analysis as initial conditions, the model fails to reproduce the decaying MCS that occurred over the network during the initial few integration hours (not shown), although this system has little impact on the later development of the squall line (see ZGP). As expected, the squall line convection is initiated a couple of hours later than in the control run; this is again a typical spinup problem. Consequently, the organization of the squall line's circulation is delayed. Nevertheless, the model simulates well the orientation and propagation of the squall line and its associated convective and grid-scale precipitation after its initiation (see Figs. 17 and 18), except that its location at 0600 UTC lags 150 km behind the observed. Vertical cross sections (not shown) indicate that the model also reproduces the RTF descending and the FTR ascending flow, as evidenced by the predicted presquall mesolows, mesohighs, and wake lows in Fig. 18, but their intensity is much weaker than that in the control run. The results indicate that frontogenesis processes would sooner or later produce organized vertical circulations (Holton 1979) that are favorable for the development of MCSs, as long as the initial conditions contain reasonable magnitudes of baroclinicity. In the present case, cold advection behind the short-

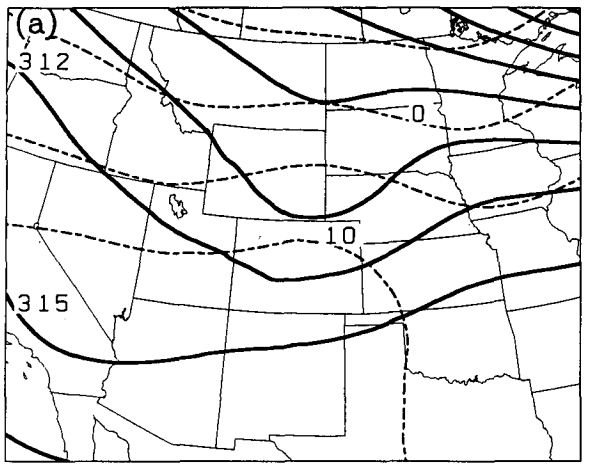

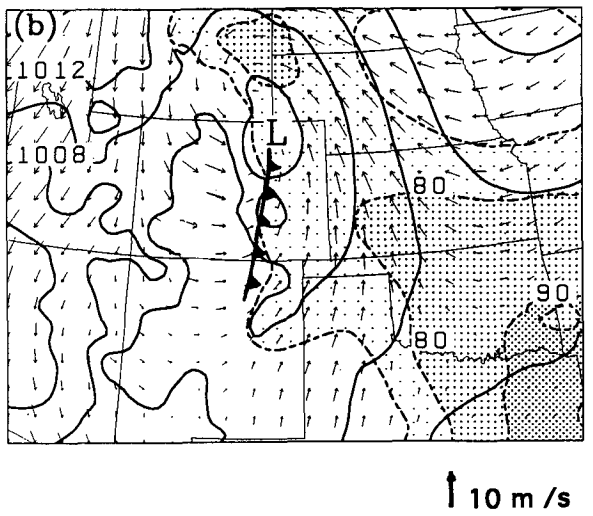

FIG. 16. As in Fig. 2 but from the CMC analysis without data enhancement.

wave trough appears to play an important role in assisting the initial spinup of vertical circulations.

Perhaps one of the most pronounced problems with this forecast is the appearance of a strong low pressure center over southeastern Nebraska. This feature can be traced back to the low pressure at the Colorado–Wyoming–Nebraska border at the initial time (cf. Figs. 2b and 16b). As can be visualized from Fig. 16, the strong cyclonic flow in combination with the pressure pattern has a strong resemblance to a typical extratropical cyclone with the squall line as the cold front part. The squall line forms along the north–south-oriented surface front and moves east with the "cyclone" system. In contrast, with the enhanced initial conditions, the low pressure center at the Colorado–Wyoming border is just a part of the frontal system and is pushed southeast by the cold air behind it. Thus, the low pressure in the control run evolves into an elongated presquall mesolow once the squall line becomes

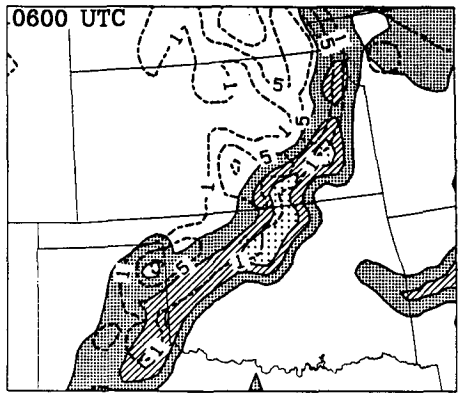

FIG. 17. As in Fig. 3i but for experiment CMC.

organized ahead of the surface front (Figs. 3d–f). In this regard, it is essential to have better-defined mesoscale details, such as baroclinic zones, moist tongues, and convergence zones in the initial conditions in order to obtain more realistic prediction of MCSs and larger-scale environments. Some recent studies have shown that model initial conditions can be readily improved if a regional data assimilation system can be developed to include all available observations (e.g., Miller and Benjamin 1992; Chouinard et al. 1994).

5. Summary and conclusions

In this study, an improved version of the operational Canadian regional finite-element (RFE) model has been used with a fine-mesh grid size of 25 km to examine the feasibility of operational prediction of an intense squall line that occurred during 10–11 June 1985. The model has been tested with different types

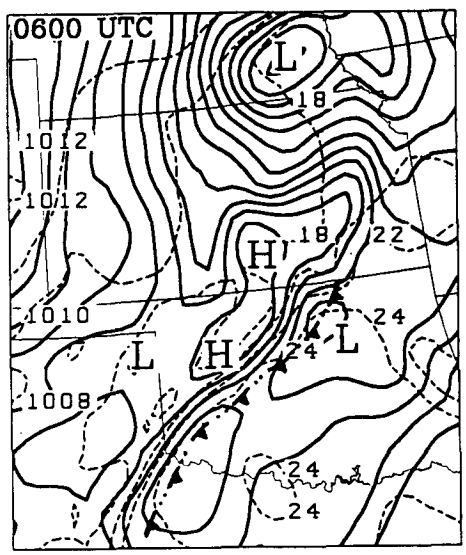

FIG. 18. As in Fig. 3f but for experiment CMC.

of condensation schemes and initial conditions. The study demonstrates the potential for the operational model to improve quantitative precipitation forecasts and severe weather warnings if realistic model physics, reasonable initial conditions, and high resolution are used. The most important conclusions of this study are briefly summarized in the following.

- In addition to focusing on smaller horizontal grid size, which will likely improve the timing and location of convective initiation, equal attention must be paid to improving the explicit moist physics and cumulus parameterizations used if one wants to better reproduce various types of meso-β-scale circulations and their associated precipitation, particularly for MCSs that develop in weak-gradient environments.
- When the Fritsch–Chappell convective parameterization and an explicit moisture scheme are simultaneously used, the RFE model reproduces remarkably well much of the observed internal structure and evolution of the squall system, such as surface mesohighs and mesolows, FTR ascending and RTF descending flows, and a cooling-induced midlevel mesovortex, even though the model is initialized with conventional observations. The predicted timing, location, propagation, and the precipitation amount and distribution of the squall system also compare favorably with the special network observations.
- When either the MCA or the Kuo scheme is incorporated, the model reproduces well the line structure of convective precipitation associated with the squall system. However, both schemes are unable to reproduce the observed internal flow structures of the system, as well as the associated surface pressure and thermal perturbations at the mature and decaying stages, owing partly to the lack of moist downdrafts. In addition, because of their inherent assumptions, the MCA scheme tends to delay the initiation of deep convection, while the Kuo scheme tends to remove too much moisture from the boundary layer such that the grid-scale precipitation is significantly underestimated. Thus, these two schemes do not appear to be suitable for being used to predict the internal structure and evolution of MCSs and their associated precipitation events.
- High-resolution initial conditions obtained from regional data assimilation systems at operational centers will have a positive impact on the successful prediction of the timing and location of MCSs, particularly when the environmental baroclinicity is weak. Poor resolution of mesoscale gradients, such as surface fronts, moist tongues, and convergence zones, may significantly alter the predicted structure and evolution of MCSs. In the present case, with a low-resolution analysis alone, the model produces a "cyclonelike" mesoscale circulation associated with the squall system.

It is important to point out that some of the above conclusions were obtained from a single case study, while others have been supported by previous numerical studies of summertime MCSs (e.g., Zhang and Fritsch 1988; Zhang et al. 1988; Zhang and Gao 1989). Whether or not they are valid for a wide range of circumstances needs to be tested with additional numerical studies of other MCSs. It should also be kept in mind that all the model results presented in this study were produced using a horizontal resolution of 25 km, which is higher than the one typically used in current operational models. Whether or not the preceding conclusions hold with a horizontal resolution of 40–50 km still needs to be verified. The research along this line is currently under way at the Montreal mesoscale community with a view to help improve operational forecasts of MCSs and their associated quantitative precipitation.

Acknowledgments. This work has been made possible through Environment Canada Contract KM156-0-9029 and a graduate fellowship from the Natural Sciences and Engineering Research Council of Canada. The authors are very grateful to Michel Béland of Recherche en Prévision Numérique/Atmospheric Environment Service for his continuing interest and generous support during the course of this project. Thanks also go to Michel Valin, Bernard Bilodeau, Monique Tanguay, André Tremblay, and Mario Lépine at RPN for their kindly assistance.

REFERENCES

Anthes, R. A., E.-Y. Hsie, and Y.-H. Kuo, 1987: Description of the Penn State/NCAR Mesoscale Model Version 4 (MM4). Tech. Note, NCAR/TN-282, 66 pp.

Arakawa, A., and W. H. Schubert, 1974: Interaction of a cumulus cloud ensemble with the large-scale environment, part I. *J. Atmos. Sci.*, **31**, 674–701.

Benjamin, S. G., and N. L. Seaman, 1985: A simple scheme for improved objective analysis in curved flow. *Mon. Wea. Rev.*, **113**, 1184–1198.

Benoit, R., J. Côté, and J. Mailhot, 1989: Inclusion of a TKE boundary layer parameterization in the Canadian Regional Finite-Element Model. *Mon. Wea. Rev.*, **117**, 1726–1750.

Biggerstaff, M. I., and R. A. Houze Jr., 1991a: Kinematic and precipitation structure of the 10–11 June 1985 squall line. *Mon. Wea. Rev.*, **119**, 3034–3065.

——, and ——, 1991b: Midlevel vorticity structure of the 10–11 June 1985 squall line. *Mon. Wea. Rev.*, **119**, 3066–3079.

Chang, C.-B., D. J. Perkey, and C. W. Kreitzberg, 1986: Impact of missing wind observations on the simulation of a severe storm environment. *Mon. Wea. Rev.*, **114**, 1278–1287.

Charba, J. P., and W. H. Klein, 1980: Skill in precipitation forecasting in the National Weather Service. *Bull. Amer. Meteor. Soc.*, **61**, 1546–1555.

Chouinard, C., J. Mailhot, H. Mitchell, A. Staniforth, and R. Hogue, 1994: The Canadian regional data assimilation system: Operational and research applications. *Mon. Wea. Rev.*, **122**, 1306–1325.

Cressman, G. P., 1959: An operational objective analysis system. *Mon. Wea. Rev.*, **87**, 367–374.

Cunning, J. B., 1986: The Oklahoma–Kansas preliminary regional experiment for STORM-Central. *Bull. Amer. Meteor. Soc.*, **67**, 1478–1486.

DiMego, G. J., K. E. Mitchell, R. A. Petersen, J. E. Hoke, J. P. Gerrity, J. C. Tuccilo, R. L. Wobus, and H. H. Juang, 1992: Changes to NMC's regional analysis and forecast system. *Wea. Forecasting.*, **7,** 185–198.

Dudhia, J., 1989: Numerical study of convection observed during the winter monsoon experiment using a mesoscale two-dimensional model. *J. Atmos. Sci.*, **46,** 3077–3107.

Fawcett, E. B., 1977: Current capabilities in prediction at the National Weather Service's National Meteorological Center. *Bull. Amer. Meteor. Soc.*, **58,** 143–149.

Frank, W. M., 1983: The cumulus parameterization problem. *Mon. Wea. Rev.*, **111,** 1859–1871.

Fritsch, J. M., and C. F. Chappell, 1980: Numerical prediction of convectively driven mesoscale pressure system. Part I: Convective parameterization. *J. Atmos. Sci.*, **37,** 1722–1733.

——, and K. F. Heideman, 1989: Some characteristics of the Limited-Area Fine-Mesh (LFM) Model quantitative precipitation forecasts (QPF) during the 1982 and 1983 warm seasons. *Wea. Forecasting,* **4,** 173–185.

——, R. A. Maddox, and A. G. Barnston, 1981: The character of mesoscale convective complex precipitation and its contribution to warm season rainfall in the U.S. Preprints, *Fourth Conf. Hydrometeorology,* Reno, NV, Amer. Meteor. Soc., 94–99.

Gao, K., D.-L. Zhang, M. W. Moncrieff, and H.-R. Cho, 1990: Mesoscale momentum budget in a midlatitude squall line: A numerical case study. *Mon. Wea. Rev.*, **118,** 1011–1028.

Gravel, S., and A. Staniforth, 1992: Variable resolution and robustness. *Mon. Wea. Rev.*, **120,** 2633–2640.

Grell, G. A., 1993: Prognostic evaluation of assumptions used by cumulus parameterizations. *Mon. Wea. Rev.*, **121,** 764–787.

Heideman, K. F., and J. M. Fritsch, 1988: Forcing mechanisms and other characteristics of significant summertime precipitation. *Wea. Forecasting,* **3,** 115–130.

Holton, J. R., 1979: *An Introduction to Dynamic Meteorology,* 2d ed. Academic Press, 391 pp.

Hsie, E.-Y., R. A. Anthes, and D. Keyser, 1984: Numerical simulation of frontogenesis in a moist atmosphere. *J. Atmos. Sci.*, **41,** 2581–2594.

Johnson, R. H., and P. J. Hamilton, 1988: The relationship of surface pressure features to the precipitation and airflow structure of an intense midlatitude squall line. *Mon. Wea. Rev.*, **116,** 1444–1472.

Kelly, G. A. M., G. A. Mills, and W. L. Smith, 1978: Impact of *Nimbus-6* temperature soundings on Australian region forecasts. *Bull. Amer. Meteor. Soc.*, **49,** 393–405.

Krishnamurti, T. N., Y. Ramanathan, H.-L. Pan, R. L. Pasch, and J. Molinari, 1980: Cumulus parameterization and rainfall rates. I. *Mon. Wea. Rev.*, **108,** 465–472.

Kuo, H. L., 1974: Further studies of the parameterization of the influence of cumulus convection on large-scale flow. *J. Atmos. Sci.*, **31,** 1232–1240.

Kurihara, Y., 1973: A scheme for moist convective adjustment. *Mon. Wea. Rev.*, **101,** 547–553.

Mailhot, J., 1992: Numerical simulation of air mass transformation over the Gulf of Mexico. *J. Appl. Meteor.*, **31,** 946–963.

——, and C. Chouinard, 1989: Numerical forecasts of explosive winter storms: Sensitivity experiments with a meso-α scale model. *Mon. Wea. Rev.*, **117,** 1311–1343.

——, and ——, R. Benoit, M. Roch, G. Verner, J. Côté, and J. Pudykiewicz, 1989: Numerical forecasting of winter coastal storms during CASP: Evaluation of the Regional Finite-Element Model. *Atmos.-Ocean,* **27,** 24–58.

Manabe, S., J. Smagorinsky, and R. F. Strickler, 1965: Simulated climatology of a general circulation model with a hydrologic cycle. *Mon. Wea. Rev.*, **93,** 769–798.

Miller, P. A., and S. G. Benjamin, 1992: A system for the hourly assimilation of surface observations in mountainous and flat terrain. *Mon. Wea. Rev.*, **120,** 2342–2359.

Mills, G. A., and R. S. Seaman, 1990: The BMRC regional data assimilation system. *Mon. Wea. Rev.*, **118,** 1217–1237.

Molinari, J., and M. Dudek, 1992: Parameterization of convective precipitation in mesoscale numerical models: A critical review. *Mon. Wea. Rev.*, **120,** 326–344.

Ramage, C. S., 1982: Have precipitation forecasts improved? *Bull. Amer. Meteor. Soc.*, **63,** 739–743.

Roch, M., R. Benoit, and N. Parker, 1991: Sensitivity experiments for polar low forecasting with the CMC Mesoscale Finite-Element Model. *Atmos.-Ocean,* **29,** 381–419.

Rotunno, R., J. B. Klemp, and M. L. Weisman, 1988: A theory for strong, long-lived squall lines. *J. Atmos. Sci.*, **45,** 463–485.

Rutledge, S. A., R. A. Houze Jr., M. I. Biggerstaff, and T. Matejka, 1988: The Oklahoma–Kansas mesoscale convective system of 10–11 June 1985: Precipitation structure and single Doppler radar analysis. *Mon. Wea. Rev.*, **116,** 1409–1430.

Sanders, F., 1979: Trends in skill of daily forecasts of temperature and precipitation, 1966–78. *Bull. Amer. Meteor. Soc.*, **60,** 763–769.

Smull, B. F., and R. A. Houze Jr., 1985: A midlatitude squall line with a trailing region of stratiform rain: Radar and satellite observations. *Mon. Wea. Rev.*, **113,** 117–133.

Staniforth, A. N., and H. L. Mitchell, 1978: A variable-resolution finite-element technique for regional forecasting with the primitive equations. *Mon. Wea. Rev.*, **106,** 439–447.

——, and R. W. Daley, 1979: A baroclinic finite-element model for regional forecasting with the primitive equations. *Mon. Wea. Rev.*, **107,** 107–121.

——, and J. Mailhot, 1988: An operational model for regional weather forecasting. *Comput. Math. Appl.*, **16,** 1–22.

Tanguay, M., A. Simard, and A. N. Staniforth, 1989: A three-dimensional semi-Lagrangian scheme for the Canadian Regional Finite-Element Forecast Model. *Mon. Wea. Rev.*, **117,** 1861–1871.

Weisman, M. L., 1992: The role of convectively generated rear-inflow jets in the evolution of long-lived mesoconvective systems. *J. Atmos. Sci.*, **49,** 1826–1847.

Zhang, D.-L., 1989: The effect of parameterized ice microphysics on the simulation of vortex circulation with a mesoscale hydrostatic model. *Tellus,* **41A,** 132–147.

——, 1992: The formation of a cooling-induced mesovortex in the trailing stratiform region of a midlatitude squall line. *Mon. Wea. Rev.*, **120,** 2763–2785.

——, and J. M. Fritsch, 1986a: A case study of the sensitivity of numerical simulation of mesoscale convective systems to varying initial conditions. *Mon. Wea. Rev.*, **114,** 2418–2431.

——, and ——, 1986b: Numerical simulation of the meso-β scale structure and evolution of the 1977 Johnstown flood. Part I: Model description and verification. *J. Atmos. Sci.*, **43,** 1913–1943.

——, and ——, 1988: Numerical sensitivity experiments of varying model physics on the structure, evolution and dynamics of two mesoscale convective systems. *J. Atmos. Sci.*, **45,** 261–293.

——, and K. Gao, 1989: Numerical simulation of an intense squall line during 10–11 June 1985 PRE-STORM. Part II: Rear inflow, surface pressure perturbations and stratiform precipitation. *Mon. Wea. Rev.*, **117,** 2067–2094.

——, and H.-R. Cho, 1992: The development of negative moist potential vorticity in the stratiform region of a simulated squall line. *Mon. Wea. Rev.*, **120,** 1322–1341.

——, E.-Y. Hsie, and M. W. Moncrieff, 1988: A comparison of explicit and implicit predictions of convective and stratiform precipitating weather systems with a meso-β scale numerical model. *Quart. J. Roy. Meteor. Soc.*, **114,** 31–60.

——, K. Gao, and D. B. Parsons, 1989: Numerical simulation of an intense squall line during 10–11 June 1985 PRE-STORM. Part I: Model verification. *Mon. Wea. Rev.*, **117,** 960–994.